PART I

FIBERS: INTERFACE AND ARCHITECTURE

CHAPTER 1

REINFORCEMENT OF CERAMIC MATRIX COMPOSITES: PROPERTIES OF SiC-BASED FILAMENTS AND TOWS

JACQUES LAMON,[1] STÉPHANE MAZERAT,[2] AND MOHAMED R'MILI[3]

[1]*Laboratoire de Mécanique et Technologie (LMT), CNRS (Centre National de la Recherche Scientifique), ENS Cachan (Ecole Normale Supérieure), UPMC (Univesité Pierre et Marie Curie), Cachan, France*
[2]*Laboratoire des Composites Thermostructuraux, Université de Bordeaux, Pessac, France*
[3]*Laboratoire MATEIS, CNRS, INSA de Lyon, Université de Lyon, Villeurbanne, France*

1.1 INTRODUCTION

Proper reinforcement of ceramics is aimed at increasing the resistance to crack propagation by introducing elements that can arrest the cracks. Only continuous fibers are able to arrest the cracks through deflection at fiber/matrix interfaces. Composite damage tolerance requires strong fibers and appropriate interfaces. Composite strength requires strong fibers and damage tolerant multifilament tows.

In continuous-fiber-reinforced ceramics, only those fibers that can withstand the high temperatures required by matrix processing (above 1000°C) can be used. Other high temperature requirements to be met include long-term stability, creep resistance, and oxidation resistance. A wide spectrum of continuous fiber–reinforced ceramic matrix composites (CMCs) can be foreseen owing to a wide variety of matrices and fibers. Non-oxide CMCs reinforced by non-oxide fibers have been the most studied. The reason for this is that carbon and silicon carbide fibers display the highest properties for use at high temperature. Second, for compatibility reasons, non-oxide fibers can be combined essentially to non-oxide matrices. However, carbon fibers degrade in oxidizing atmosphere at temperatures as low as 450°C, and they must be protected. SiC-based fibers are much more resistant to oxidation. Oxide fibers are inherently resistant to oxidation, but they have limited creep resistance and undergo grain growth at high temperatures, which causes strength degradation. Further, they display much higher densities than carbon and SiC-based fibers. Despite these drawbacks, alumina-based CMCs have been extensively studied.

The literature abounds in papers, book chapters, and books on microstructure/properties relationships for oxide and non-oxide fibers [1–4]. Carbon fibers are discussed in another chapter of this book. The present chapter focuses on a recent important issue for continuous SiC-based reinforcing ceramic fibers that has been ignored because potential use of CMCs was driven by their superior temperature resistance over metals. Use at very high temperatures above 1000°C was essentially foreseen. Recently, a growing interest was fostered by lightweight features of CMCs for use in the range of allowable temperatures for metals (below 1000°C in aeronautical engines).

Ceramic Matrix Composites: Materials, Modeling and Technology, First Edition. Edited by Narottam P. Bansal and Jacques Lamon.

The Nextel oxide fibers are the most widely used reinforcements for continuous fiber oxide–oxide composites [5–7]. Nextel 610 fiber has the highest strength and elastic modulus (3.1 GPa and 380 GPa, respectively), but it is limited by creep to temperatures <1000°C. Nextel 720 fiber has lower room temperature strength (2.1 GPa), but higher creep resistance, which allows use at higher temperatures (up to 1200°C). Sapphire (single crystal Al_2O_3) fibers are no longer available, their cost and diameter (>50 μm) limit their use in composites.

Non-oxide fibers exhibit superior tensile strength and creep resistance to the oxides. They possess comparable Young's moduli and diameters. Table 1.1 lists the main properties of SiC-based ceramic fibers [1,2,8–29]. Lower creep rates are observed at temperatures >1200°C, even under high stresses, whereas the oxide fibers can barely exceed 1000°C [1, 3, 30–35]. For example, Sylramic SiC fibers show less than 1% creep strain after 1000 hours at 1350°C and 100 MPa stress, or Hi-Nicalon type S fibers show less than 0.5% creep strain after 60 hours at 1350°C and 850 MPa stress. Creep strain of 10^{-8} per second is obtained at 1000°C and 100 MPa stress on the most creep-resistant oxide fiber (Nextel 720), at 1400°C and 300 MPa stress on Tyranno SA3, and at 1350°C and 850 MPa on Hi-Nicalon type S. Tyranno SA3 and Hi-Nicalon type S exhibit higher resistance to creep than Hi-Nicalon. The creep resistance is commensurate with low oxygen content, SiC grain size, and small amount of amorphous phase. It has been shown to be improved after high temperature treatment under various atmospheres. Creep behavior of Hi-Nicalon can be improved by using high temperature treatment that eliminates amorphous phase and organizes better carbon structure [3].

1.2 PROCESSING OF SiC-BASED FILAMENTS

Three generations of SiC-based fibers were manufactured essentially by two companies: Nippon Carbon Co. Ltd. and UBE INDUSTRIES Ltd. They differ by composition and properties as a result of the organosiliced precursors and manufacturing processes used (Table 1.1).

Fibers of the first generation (NicalonTM (Nicalon NLP101, NLM202, NLM207) and Tyranno (Tyranno ZMI, LOX-M, S, AM) Si-O-C fibers) were spun from a molten polycarbosilane (PCS) based ceramic precursor, cured under oxygen around 180°C during about 1 hour, and then submitted to a pyrolysis treatment under an inert gas, giving rise to a fine diameter SiC-based fiber [36,37]. The first ones NLM 101 and NLM 200 have been commercialized since the late 1970s by Nippon Carbon Co., Yokohama, Japan (NC).

All these fibers contain a large amount of oxygen combined into amorphous silicon oxycarbide phases that are thermodynamically instable and decompose beyond 1100°C with a SiO(g) and CO(g) evolution and SiC crystal growth. This decomposition yields significant strength degradation [23, 29, 38–41].

For the Tyranno family fibers, a precursor resulting from the reaction of PCS with an alkoxide (M = Ti, Zr, or Al) was used [18, 19]. These Si-M-C-O Tyranno fibers containing metal additives show improved thermal stability and chemical corrosion resistance, and the degradation occurs at higher temperature (>1300°C) when compared with the Si-C-O Nicalon fibers [17, 42].

To avoid thermal instability due to presence of the oxycarbide phase, a nearly oxygen-free SiC fiber (Hi-Nicalon fiber from Nippon Carbon) was developed in 1990 by melt spinning, electron beam curing, and pyrolysis of PCS precursor under anaerobic conditions [15, 43]. This fiber exhibits much better thermal stability than the standard Nicalon fiber; however, it also contains a large excess of turbostratic carbon, which affects resistance to oxidation and creep [3, 4, 8, 44].

To reduce the free carbon content and to improve the high temperature properties of the fibers, near pure SiC fibers were produced [1, 14, 45]. Those third-generation fibers include the Hi-Nicalon type S fibers [42], Tyranno SA3 fibers [43], and Sylramic fibers [16].

The Hi-Nicalon S fiber process is similar to that of Hi-Nicalon one except the thermal treatment at high temperature under hydrogen [45]. The Hi-Nicalon S fiber consists of β-SiC sub-micrometer crystals with traces of carbon and oxygen [46]. This fiber exhibits a high Young's modulus, a high creep and oxidation resistance, and an excellent thermal stability up to 1600°C [1, 14, 47].

The Tyranno SA3 fiber was obtained by heat treatment of the amorphous AM fiber at about 1800°C. It shows no significant degradation in strength or change in composition on heating up to 1800°C in argon (1 hour) and up to 1000 hours in air at 1000°C [1, 14, 48].

The Sylramic fiber is no longer produced but it is similar to the Tyranno SA3 fiber. It was manufactured from Lox-M fiber heat-treated in boron oxide environment at high temperature in order to help sintering, to decrease the oxygen content, and to obtain a finely crystallized pure SiC fiber [1, 13, 49].

TABLE 1.1 Physical Properties and Composition of Various SiC-Based Fibers [1,2,8–29]

Fiber	Diameter (μm)	Fibers/fil	Curing	$T_{pyrolyse}$ (°C)	Composition (at. %) Si	C	O	Hetero-element	C_{libre} (at. %)	<SiC-β> (nm)	σ (S/m)	$\alpha \times 10^{-6}$	Density (g/cm^3)
NL101	15 [23]	500	ox	1200	36.4 41.1	46.8 43.3	16.7 15.6	–[22] –[1]	18.8 [22] 10.0 [1]	1.2 [22] 1.1 [23]	0.02 [28]	3.1 [29]	2.57 [21]
NL102	15 [23]	500	ox	1200	33.9 35.0	48.8 51.4	17.3 13.6	–[22] –[1]	23.6 [22] 23.3 [1]	1.7 [23]		3.1 [29]	2.61 [21]
NL207	14 [11]	500	ox	>1200 [1,8,10]	38.6 37.4	48.6 49	12.8 13.6	–[22] –[1,10]	16.4 [22] 18.4 [1,10]	1.9 [22] ~2 [10,11,13]	0.006 [28] 0.1–0.01 [15,25,27] 0.005 [17]	3.2 [1,15]	2.55 [1,10,11, 13,15,17] 2.58 [21]
Hi-Ni	14 [8] 12 [1]	500	e$^-$	1300 [1] 1500 [12]	39 41.6 41.9	60.4 57.8 57.2	0.6 0.6 0.9	–[1,8,13] –[21]	21.7 [1,8,13] 15.8 [22]	5 [8,12,13]	23 [28] 71 [25] 80 [27]	3.5 [1]	2.74 [1,10,11,13,15]
Hi-Ni-S	13 [14]	500	e$^-$	>1500	48.2 48.7	50.8 51.0	1.0 0.3	–[22] –[1,9,13,14]	3.1 [22] 2.6 [1,9,13]	50 [11–13]	0.14 [2,8,27]		3.05 [1,13,14] 3.10 [9]
T-S	11 [13] 8.5 [13]	800 1600	ox		31.6 31.8	41.7 48.1	26.0 19.4	(Ti) 0.7 [21] (Ti) 0.7 [22]	23.0 [21] 26.0 [22]	1.2 [22]	0.09 [28]	3.1 [24]	2.35 [21,24]
Lox-M	8.5 [13] 11 [13]	800	ox	1200 [1] 1300 [12]	35.4 35.8 36.9	53.3 49.0 50.4	10.4 14.4 11.9	(Ti) 0.9 [22] 0.8 [1,10,13] 0.8 [17]	23.1 [22] 20.4 [1,10,13] 19.5 [17]	1.9 [22] 1.4 [18]	2.6 [28] 3.3 [17]	3.1 [1]	2 37 [10,11,13] 2.48 [1,9,17,19,24]
Lox-E	11 [1]	800	e$^-$	1300 [12]	35.7 36.4	57.0 57.8	6.6 5.8	(Ti) 0.7 [1,10,17] –[9]	24.6 [1,10] 24.3 [9]	2 [10]	125 [17] 40 [27]		2.39 [10,11,13] 2.55 [9,17]
ZMI	11 [24]	800	ox	1300	35.5 37.3	54.3 53.7	10.0 8.8	(Zr) 0.2 [22] 0.2 [10]	23.9 [22] 20.7 [10]	2.2 [22] 2.0 [18]	16 [28] 50 [25]	4.0 [19,24]	2.48 [10,18,21,24]
ZM	11 [1]	800	ox	1300 [1] 1550 [17]	34.7 37.7	56.5 53.4	8.6 8.7	(Zr) 0.2 [21] 0.2 [1,17]	26.0 [21] 20.5 [1]	2.48 [22] ~2 [17]	47 [28] 50 [17]		2.48 [1,13,17]
ZE	11 [1]	800	e$^-$	1300 [1] 1580 [17]	36.3 38.7	61.9 59.1	1.7 2.0	(Zr) 0.1 [21] 0.2 [1,13,17]	26.4 [21] 21.4 [1,10]	3.5 [22]	380 [28] 330 [17,25]		2.55 [1,10,17]
ZX	11 [19]	800	ox	1500 [19]	37.0 34.8	53.7 52.9	9.1 12.1	(Zr) 0.2 [19] 0.2 [19]	21.2 [19] 24.1 [19]	~2 [19]			2.48 [19] 2.42 [19]
AM	11 [18] 8.5	800 1600	ox	1500 [18]	32.9 34.6	52.5 51.3	14.2 13.7	(Al) 0.4 [22] 0.4 [9,18]	26.7 [22] 23.5 [9,18]	2.2 [22] 1.8 [18]	0.15 [28]		2.42 [9,18]
SA3	10 [11] 7.5 [24]	800/1600	ox	AM+1700 + >1800 [9,12,13,18]	47.8	52.4	0.3	(Al) 0.5 [1,9,13,14]	4.75 [1,9,13]	300 [13] >200 [12]	80 [28] 660 [26]	4.5 [24]	3.02 [9,13] 3.1 [1,24]
Sylramic	10 [1]	800	ox	Lox-M + 1600 [13] or >1700 [1]	46.4	47	1.2	(Ti/B/N) 0.8/4.0/0.6 [1,13,14]	1.2 [1,13]	200 [13] 60–90 [20]	100 [26]	5.4 [1] 5.3 [20]	3.05 [1,11,13,16]

ox: cured by heating in air; e$^-$: cured by means of electron beams

1.3 FRACTURE CHARACTERISTICS OF SINGLE FILAMENTS

Fibers are brittle ceramics. The tensile behavior is completely described by Young's modulus and stress and strain at failure.

Fracture toughness, which measures the resistance to crack propagation, is difficult to measure using notched specimen-based conventional fracture mechanics techniques. However, Morishita and coworkers created a notch on a SiC Tyranno-SA3 fiber using a focused-ion beam (FIB) [50]. In most cases, available fracture toughness data are derived from diameters of fracture-inducing flaws identified by fractography in the fracture surface, using the conventional fracture mechanics equation: $K_{IC} = \sigma_r \ Y\sqrt{a_c}$, where Y is a geometrical factor characteristic of flaw shape and a_c is the critical flaw size. Fiber failure stress σ_r is either measured during the test or estimated from fracture mirror size. SiC-based fibers exhibit high resistances to failure and very low toughness (Table 1.2) [8–12, 14–21, 24]. Toughness estimates are in the range 1–2 MPa $m^{0.5}$ for most SiC fibers. Values close to 3 MPa $m^{0.5}$ have been measured on Sylramic fibers and on notched SiC Tyranno SA3 fibers. Tensile strengths and strains-to-failure reported in the literature range, respectively, between 1500 and 3500 MPa and between 1% and 1.9%. Values measured on significant batches of filaments with identical gauge length of 25 mm span comparable range (Table 1.3). Low toughness and high strengths are indicative of high sensitivity to fracture-inducing flaws and the presence of very small fracture-inducing flaws (submicron size). These features inherent to ceramic fibers reflect a scale effect. Flaw size is commensurate with fiber small dimensions and microstructure: a few microns large diameter (typically around 10 μm, Table 1.1) and fine grain size (a few nanometers).

However, it is worth emphasizing that the high strengths reported in Tables 1.2 and 1.3 are average values. They are approximate estimates depending on the number of data they average. Strength and strain data exhibit a wide variability as a result of inherent variability in failure origins, and also of uncertainties introduced by practical difficulties in the determination of fiber diameter (enhanced by diameter variation along fiber) and in the direct measurement of deformations. During tensile tests, deformations are derived from the displacement of load train. Correction for load train compliance is necessary. It is based on a calibration technique [51]. The estimation of strength from failure load is affected by uncertainty in fiber cross-sectional area or in strain. Practically much effort is done to improve accuracy in the determination of strengths, using up-to-date measurement techniques or by testing multifilament tow specimens, as discussed in section 1.4. It is thus reasonable to consider that strength variability is dominated by the distribution of fracture-inducing flaws. The scatter is generally very wide: from 500 to 3000 MPa and 0.2–1.2% for Nicalon fibers.

1.3.1 Statistical Strength Distributions

As usual with brittle ceramics, fracture data of single filaments exhibit a significant scatter, since inherent flaws with a random distribution induce fracture. An important consequence is that the fracture stress is not an intrinsic characteristic. It is instead a statistical variable, which depends on several factors including the stress state, the size of test specimens, and the number of test specimens [52]. Therefore, a unique reference value of fracture strength cannot be recommended.

1.3.2 Weibull Distribution of Failure Strengths

It is widely accepted that the Weibull model satisfactorily describes the statistical distribution of failure strengths of single filaments under tensile loads:

$$P = 1 - \exp\left\{-\int (\sigma/\sigma_0)^m \, dV/V_0\right\} \tag{1.1}$$

where P is the probability of failure, σ is the stress, σ_0 is the scale factor, m is the Weibull modulus, V is the volume of specimen, V_0 is a reference volume ($V_0 = 1$ m^3 should be preferred), and σ_0 is related to the mean value of strength. The Weibull modulus reflects the scatter in strength data.

The strength for given size and stress state can be determined using Equation (1.1) when proper m, σ_0, and associated V_0 are known. If V_0 is not specified, the estimate of σ_0 is meaningless; the strength cannot be determined safely.

TABLE 1.2 Elastic and Failure Characteristics of Various SiC-Based Fibers

Fiber	σ_r (MPa)	E (GPa)	ε_r (%)	Weibull modulus	σ_1 (MPa)	K_{IC} (MPa $m^{1/2}$)
NL101	1840 [23] 2200 [21]	134 [24] 180 [21]	1.4 [24] 1.2 [21]	2.3 [24] 4.3 [21]	2400 [21]	1.2 [21]
NL102	1490 [24] 2600 [21]	144 [24] 180 [21]	1.0 1247 1.4 [21]	2.7 [24] 7.6 [21]	2700 [21]	1.2 [21]
NL207	2800 [21] 2700 [8] 3000 [1, 13, 15]	210 [21] 220 [13, 15] 200 [1]	1.3 [21] 1.0 [13] 1.5 [1, 15]	5.0 [21] 4.3 [21]	3100 [21] 2900 [21]	1.2 [21] 0.9 [8] 2 [1]
Hi-Ni	3000 [21] 2800 [1, 13–15, 20]	300 [21] 270 [1, 9–11, 13, 15, 20]	1.0 [8, 10, 11, 13, 15, 19–21]	9.8 [21] 5.0 [25]	3300 [21] 2880 [25]	1.7 [21]
Hi-Ni-S	2900 [21] 2600 [9] 2500 [13, 14]	420 [9] 400 [1, 13, 14]	0.6 [9, 13, 14, 21]	8.4 [21] 4.5 [25]	3000 [21] 1330 [25]	1.9 [21]
TS	3200 [21] 3300 [24]	180 [21] 170 [24]	1.8 [21] 1.9 [24]	5.9 [21]	3400 [21]	1.7 [21]
TS11	2800 [21]	180 [21]	1.5 [21]	4.8 [21]	3000 [21]	1.1 [21]
Lox-M	3000 [21] 3300 [9, 17, 24] 2500 [13] 3200 [20]	200 [21] 187 [1, 9, 13, 17, 24] 180 [20]	1.5 [21] 1.8 [9, 17, 20, 24] 1.4 [13]	4.6 [21]	3300 [21]	1.1 [21]
Lox-E	3000 [21] 3400 [9, 17] 2900 [1, 13]	200 [21] 206 [9 17] 200 [1, 13]	1.5 [21] 1.7 [9, 17] 1.4 [1, 11]	5.5 [21]	3200 [21]	1.0 [21]
ZMI	3100 [21] 3400 [9, 10, 18, 24]	210 [21] 200 [9, 10, 18, 24]	1.5 [21] 1.7 [9, 10, 18, 24]	4.8 [21]	3400 [21]	0.7 [8] 1.0 [21]
ZM	3400 [1 17 21]	220 [21] 200 [1, 17]	1.6 [21] 1.7 [1, 17]	5.3 [21]	3700 [21]	1.0 [21]
ZE	3300 [21] 3500 [9, 10, 17]	230 [1, 9, 10, 17, 21]	1.4 [21] 1.5 [9, 10, 17]	5.7 [21]	3500 [21]	1.3 [21]
ZX	3000 [19]	195 [19]	1.5 [19]			
AM	2800 [8, 21]	180 [9, 18, 21]	1.6 [9, 18, 21]	6.2 [21]	3000 [21]	1.2 [21]
SA3	2800 [9, 13, 14, 24] 2500 [11]	420 [9] 330 [11] 375 [1, 13, 24] 303 [13]	0.7 [9, 24] 0.75 [11] 1.45 [13] 0.9 [13]			
Sylramic	3000 [11, 13] 3200 [10, 13] 2800 [20]	390 [11] 400 [1, 13, 20] 372 [9, 10, 13]	0.8 [1, 13, 14] 1.7 [20]	4.6 [20]		3–3.5 [20]

It is important to stress that the estimate of σ_0 depends on dimension units [52]. For instance, the σ_0 estimates are substantially different if V_0 is set to 1 m^3 or 1 mm^3 as shown by Equation (1.2) derived from Equation (1.4) given in the next section for a uniform uniaxial stress state:

$$\sigma_0(\mathrm{m}^3) = \sigma_0(\mathrm{mm}^3)\{V_0(\mathrm{mm}^3)/V_0(\mathrm{m}^3)\}^{1/m} = \sigma_0(\mathrm{mm}^3)10^{-9/m} \tag{1.2}$$

where σ_0 (m^3) and σ_0 (mm^3) are estimates corresponding, respectively, to V_0 (m^3) and V_0 (mm^3).

TABLE 1.3 Failure Characteristics Measured on Various SiC-Based Filaments Under Identical Conditions (Gauge Length 25 mm) [21]

Fibers	Nb of specimens	$\sigma_r \pm$ std dev (MPa)	m	σ_l (MPa)	σ_0 (MPa)
NL101	50	2166 ± 559	4.28	2391	5.5
NL102	50	2563 ± 422	7.64	2720	87.2
NL202			5.5	2270	19
NL207	100	2839 ± 667	5.05	3090	16.7
Hi-Ni	49	3136 ± 368	9.84	3295	225.5
Hi-Ni-S	44	2877 ± 414	8.42	3062	129.2
TS	72	3152 ± 624	5.90	3413	35.4
TS11	40	2776 ± 647	4.79	3034	11.5
Lox-M	44	2984 ± 695	4.63	3314	9.9
Lox-E	41	2939 ± 582	5.54	3238	25
ZMI	49	3076 ± 742	4.81	3372	12.8
ZM	46	3439 ± 751	5.29	3688	23.6
ZE	50	3250 ± 683	5.69	3521	32.16
AM	91	2816 ± 534	6.15	3031	40.4

Except for the Nicalon NL202 Fiber, σ_l was Estimated Since Fiber Diameters were not Measured Before Tests, and σ_0 ($V_0 = 1$ m^3) was Derived from σ_l using Equation (1.3) and Average Diameters given in Table 1.1. For the NL202 Fiber, σ_0 was Estimated from Test Data, Fiber Diameters were Measured Before Tests using Laser Diffractometry [53]. σ_l was Derived from σ_0.

Authors assume implicitly that the sectional area is identical in all the fibers when they use instead a characteristic strength ($\sigma_\mathbf{l}$) that is associated to a characteristic length (Equation 1.5). σ_0 is related to the characteristic strength by the following equation derived from Equations (1.4) and (1.5):

$$\sigma_0(\mathrm{m}^3) = \sigma(\mathrm{mm})\{V(\mathrm{mm}^3)L_0(\mathrm{mm})/V_0(\mathrm{m}^3)\}^{(1/m)} \tag{1.3}$$

$\sigma_\mathbf{l}$ is the characteristic strength for gauge length L, V is the volume for L, and $L_0 = 1$ mm. The values of Weibull modulus of most SiC-based fibers are rather small (Tables 1.2 and 1.3). They span a range from 2.3 to 9.9. A significant scatter in m estimates is generally observed for each fiber: for instance, m ≅ 2.3–7.1 is reported for Nicalon fibers [53–55]. The variation is inherent to the use of an estimator to construct the Weibull plot, to the use of limited sample size, and to the selection of sample [56]. Tables 1.2 and 1.3 also report the scale factors estimated for various SiC fibers. Because of lack of uniformity in treatment of test data in the literature, only those scale factors obtained in comparable conditions were kept. Table 1.3 reports σ_0 values that were derived from characteristic strengths σ_l for the average diameters given in Table 1.1. For the Nicalon NL202 fibers, σ_0 value was determined on single filaments for which diameters were measured before the tests. σ_l was calculated from σ_0. These data are given for information. Potential users should be reminded that when the diameter is neglected, the scale factor might be affected by variability in fiber diameter. It is clear that the σ_0 estimates obtained for diameters measured on each fiber are the most pertinent.

1.3.3 Determination of Weibull Statistical Parameters

For a single gauge length and uniform tensile stress, Equation (1.1) reduces to

$$P = 1 - \exp - \left[\frac{V}{V_0}\left(\frac{\sigma}{\sigma_0}\right)^m\right] \tag{1.4}$$

or to Equation (1.5), when the sectional area is neglected to be constant:

$$P = 1 - \exp -[(\sigma/\sigma_0)^m 1/L_0] \tag{1.5}$$

The Weibull modulus m is obtained by fitting Equation (1.4) to the distribution of experimental strength data or as the slope of the "Weibull plot" of ln (ln(1/1−P)) vs. ln σ. The scale factor σ_0 is determined from the ordinate at origin k:

$$\ln(\ln(1/1-P)) = m\ln\sigma + k \tag{1.6}$$

Either graphical or curve-fitting methods (like linear regression analysis, least squares method, or maximum likelihood estimator) can be used [52].

The Weibull plot is constructed, using an estimator for estimation of failure probabilities associated to failure data ranked in ascending order. Various estimators have been devised in the literature [52]. The estimator $P_j = j/N$ can be used on large sample sizes. The estimator $P_j = (j-0.5)/N$ is recommended for limited sample sizes (>30 specimens); j is the rank of filament strength, N is the total number of data.

Another method of determining Weibull modulus is to measure fiber strength as a function of gauge length. With increasing gauge length, the chance of finding a large flaw increases, so fiber strength decreases. The effect of gauge length is given by the equation:

$$\ln\sigma = -1/m\ln L + k' \tag{1.7}$$

where L is gauge length and k' is a constant. Thus, the slope of a log–log plot of strength vs. gauge length is $-1/m$.

1.3.4 Normal Distribution

The normal distribution should be a natural solution. It is considered the most prominent probability distribution in statistics. It indicates the probability of occurrence of a characteristic in a population of infinite size. Then, certain distributions can be approximated by the normal distribution when the sample size is large (e.g., the binomial distribution, the Poisson distribution, the chi-squared distribution, the Student's t-distribution). It is reported that this trend is also observed with the Weibull distribution when the shape parameter $3 \le m \le 4$ [57]. The Normal distribution is not used in fracture statistics. It has been assumed by a few researchers for the distribution of strengths in the locality of flaws [58,59]. It has been demonstrated recently on SiC Nicalon fibers that flaw strengths follow normal distribution [56]. For the demonstration, large sets of 500 and 1000 strength data were used. Effort was devoted to the elimination of sources of variability. The analysis was based on strain-to-failure, which allowed elimination of the influence of fiber diameter on fiber strength. Strains were measured using an extensometer clamped to test specimens, which consisted of tows of 500 or 1000 filaments. A lubricant was introduced to avoid interfiber friction. Filament failures were detected from acoustic emission.

Equations of Gaussian probability density function f(ε) and normal distribution $P_N(E < \varepsilon)$ are

$$f(\varepsilon) = \frac{1}{S\sqrt{2\pi}}\exp\left[-\frac{(\varepsilon-\mu)^2}{2S^2}\right] \tag{1.8}$$

$$P_N(E \le \varepsilon) = \int_0^{\varepsilon} f(\varepsilon)d\varepsilon \tag{1.9}$$

where ε is the strain to failure, μ is the mean, and S is the standard deviation.

The probability density function derived from acoustic emission monitoring is a bell curve described by a Gaussian function, symmetric about its mean (Figure 1.1). Quite identical parameters μ and S were estimated on three bundles of Nicalon filaments (Table 1.4).

The corresponding normal distribution coincides with the Weibull distribution function (Equation 1.4) for the statistical parameters reported in Table 1.4 (Figure 1.2). The scatter in Weibull scale factors is quite negligible. The shape parameter values (5.23–5.43; Table 1.4) show a very small variation when comparing to the data reported in the literature: 2.3–7.1 [53 and 55]. Referring to the limited scatter in Weibull parameters that was obtained, and to the large size of the data samples that were analyzed, it is considered that these data approach the true statistical parameters.

The Gaussian probability density function shows the presence of a single population of fracture-inducing flaws, while volume- and surface-located flaws have been observed by Scanning Electron Microscope (SEM) fractography [53]. It confirms previous results, which showed that the contributions of the populations of surface- and volume-located flaws cannot be separated [53].

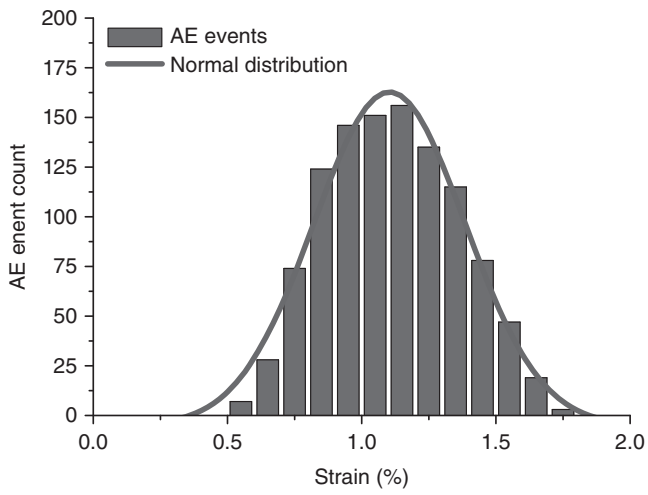

FIGURE 1.1
Histogram of filament strengths described by the distribution of AE events during a tensile test on a bundle of 1000 Nicalon SiC filaments. Reprinted with permission from APS.

TABLE 1.4 Statistical Parameters of Normal and Weibull Distributions of Flaw Strengths for Nicalon Filaments

		Normal distribution		Weibull distribution			
Test specimen	Number of filaments	μ(%)	S(%)	m	ε_l(%)	ε_0(%)	σ_0(MPa)
1	487	1.16	0.25	5.30	1.25	0.01	23.4
2	986	1.11	0.24	5.23	1.20	0.01	21.1
3	924	1.15	0.24	5.43	1.23	0.01	25.7

$V_0 = 1\ m^3$.

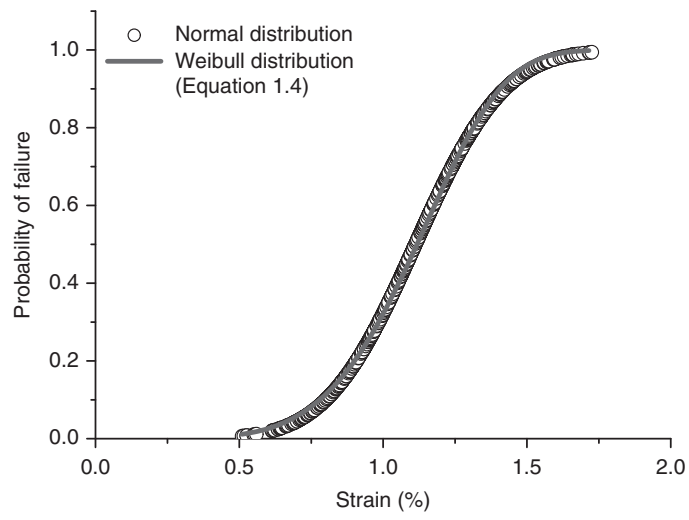

FIGURE 1.2
Cumulative distribution functions of filament failure strains obtained on a Nicalon SiC fiber bundle: Normal distribution vs. Weibull distribution (Equation 1.4). Reprinted with permission from APS.

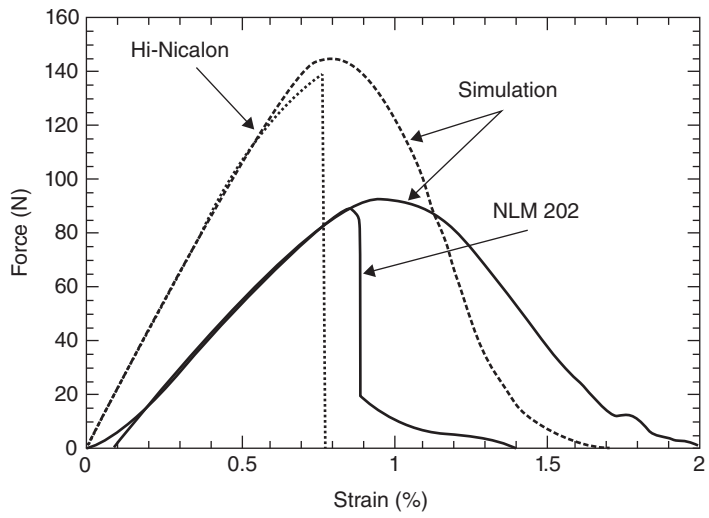

FIGURE 1.3
Ideal tensile behavior of SiC tows obtained under conditions of equal load sharing and parallel and independent filaments, and behavior obtained experimentally. Reprinted with permission from Elsevier.

1.4 MULTIFILAMENT TOWS

Multifilament tows represent a fundamental entity in composites reinforced with fabrics. They comprise several hundreds or thousands of single filaments. They progressively carry the load as the matrix is damaged, and they control ultimate failure [60]. Multifilament tows are elastic and damage tolerant, whereas single fibers are brittle.

Two different tensile behaviors are observed depending upon loading conditions and fiber (Figure 1.3) [61]:

- either a nonlinear force–strain relation resulting from successive individual fiber breaks under controlled deformation rate. This ideal behavior is obtained on carbon fiber tows or on certain SiC-based fiber tows with a lubricant (like SiC Nicalon). A typical force–strain curve together with locations of acoustic emission events in the gauge length is shown in Figure 1.4. The curve displays the conventional features of bundle tensile behavior, that is, initial elastic deformations for strains <0.5%, and then nonlinear deformations and stable failure as a result of individual successive fiber breaks as indicated by acoustic emission events.
- or a two-step nonlinear force–strain relation (Figure 1.4) under controlled deformation or load rate. After the initial elastic step, stable failure ends at maximum load. Instability results from the catastrophic failure of the filaments unbroken during the stable step. It is favored by interfiber friction. It is observed even in the presence of a lubricant on those fibers with a rough surface, associated to a large grain microstructure, like the Hi-Nicalon fibers. By contrast, the Nicalon fiber tows with fine grain microstructure (a few nanometers) exhibit a stable behavior when interfiber friction is reduced with a lubricant.

The fraction of fiber fractures at maximum force in both types of tow response controls the failure of composites. It takes the critical value $\alpha_c = N_c/N_0$, with N_0 the initial number of intact fibers, N_c the number of broken fibers at maximum load. The particular fiber that fails at maximum load is referred to as the "critical fiber." It has rank N_c, when filament strengths are ordered from smallest to largest. The fraction α_c can be satisfactorily estimated using the following relationship:

$$\alpha_c = 1 - \exp(-1/m) \tag{1.10}$$

α_c = 12–17% for Nicalon and Hi-Nicalon fiber tows, and, more generally, for those fibers with Weibull modulus $5 < m < 8$.

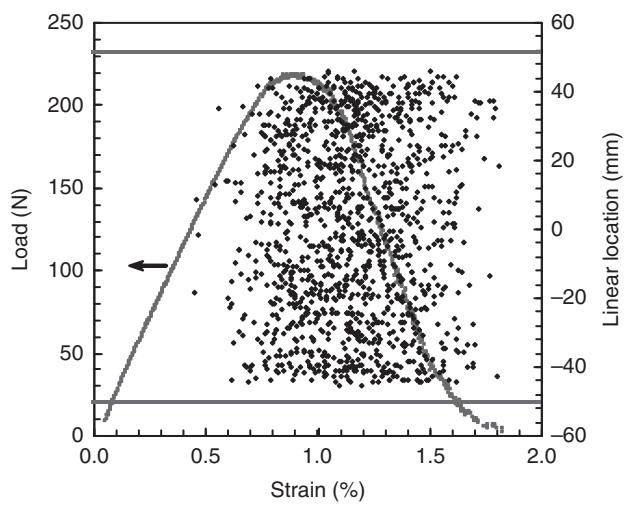

FIGURE 1.4

Load–strain curve and linear location of AE events for a Nicalon fiber bundle with a lubricant. Solid parallel lines delineate the gauge length (115 mm). Reprinted with permission from APS.

The initial number of intact filaments needs to be determined because it generally differs from the number provided by vendors, since some filaments are broken during specimen preparation. The number N_0 is derived from the initial tow compliance:

$$N_0 = N_t L_0 / E_f C_0 S_t \tag{1.11}$$

Where N_t is the total number of filaments in tow including those broken during handling or specimen preparation, L_0 is the initial gauge length, E_f is filament's Young's modulus, C_0 is the initial tow compliance, and S_t is total tow cross-sectional area.

Table 1.5 provides failure characteristics measured under monotonous tensile loading on tows of various SiC fibers. Tow strength is derived from the maximum force using the following equation:

$$\sigma_F = F_{max} / S_0 (1-\gamma)(1-\alpha) \tag{1.12}$$

where γ is the fraction of fibers broken prior to testing, $\gamma = 1 - N_0/N_t$; cross-sectional area is derived from tow mass $S_0 = m_0/L_0\rho$, ρ is density, m_0 is mass, and L_o is tow length.

TABLE 1.5 Failure Characteristics Measured on Tows for Various SiC Fibers (Gauge Length = 25 mm)

	$\sigma_F(\gamma, \alpha_c)$ (MPa)	F_{max} (N)	$\bar{\gamma}$(%)	$\bar{\alpha}_c$(%)	ε_r(%)	C_0(μm/N)
NL101	970	57	15 ± 13	10	0.84	1.6
NL207	940	60	20 ± 6.0	9.0	0.60	0.60
Hi-Ni	2100	120	14 ± 12	12	0.93	1.6
Hi-Ni-S	1800	82	25 ± 16	10	0.80	1.3
TS	1400	100	16 ± 11.2	7.3	1.1	0.90
TS11	1300	87	10 ± 8.5	10	0.98	1.6
Lox-M	1500	95	25 ± 8.1	4.5	1.0	0.80
ZMI	1400	110	14 ± 8.5	4.3	0.90	1.2
ZMId	1000	57	25 ± 6.5	3.4	0.71	0.68
AM	850	60	13 ± 11	4.9	0.71	1.1

$\sigma_F()$ is Tow Strength, F_{max} is the Maximum Force, γ is the Fraction of Filaments Broken Prior to Testing, C_0 is the Initial Compliance.

Several authors have modeled relationships between tow tensile behavior and fiber properties. H. E. Daniels [62] considered tows containing parallel and noncontacting fibers. He demonstrated that tow strengths are described by a normal distribution for large numbers of fibers. Coleman [63] proposed a relationship between tow and fiber strengths and evidenced a significant drop in tow strength when comparing to mean fiber strength. S. L. Phoenix and H. M. Taylor [64, 65] introduced effects of nonuniform loading resulting from fiber misalignment and scatter in fiber lengths within tows. V. Calard and J. Lamon [61] introduced random load sharing. They predicted tow strength drops caused by filament interactions.

1.4.1 The Bundle Model

The bundle models are based upon the following hypotheses [62, 63]: the bundle contains $N_t(= N_0)$ identical and parallel fibers (radius R_f, length l), and the statistical distribution of fiber strengths is described by the Weibull model (Equation 1.4).

When a fiber fails, equal load sharing is assumed. This means that the load is carried equally by all the surviving fibers, whereas the broken fiber no longer carries any load.

Under load-controlled conditions, the load that was carried by the broken fiber is shared equally by the surviving fibers, which experience overloading by an increment $\Delta\sigma_i$:

$$\Delta\sigma_i = \frac{\sigma_i}{N - N_i} \tag{1.13}$$

where i designates the fiber that failed, σ_i is the stress that was operating on this fiber before failure, and N_i is the number of broken fibers. Ultimate failure occurs when $\Delta\sigma_i > \sigma_{i+1} - \sigma_i$, where σ_{i+1} is the strength of the fiber having rank $i + 1$, the strengths being in ascending order. At this stage, the surviving fibers are generally unable to withstand the load increment $\Delta\sigma_i$. Most of them fail catastrophically. Failure becomes unstable at maximum load.

Under strain-controlled conditions, there is no overloading of surviving fibers when a fiber fails: $\Delta\sigma_i = 0$. As a consequence, failure is a stable phenomenon.

The ratio $\alpha(\sigma)$ of the number of broken fibers N to the initial number of fibers $N_t(= N_0)$ is approximately equal to failure probability when N_t is large and when fiber failures are equally probable events:

$$\alpha(\sigma) = \frac{N}{N_t} = P(\sigma) \tag{1.14}$$

Consequently, the total force F (σ) applied to the bundle is

$$F(\sigma) = N_t(1 - \alpha(\sigma))S_f\sigma = N_f S_f \exp - \left[\frac{V}{V_0}\left(\frac{\sigma}{\sigma_0}\right)^m\right] \tag{1.15}$$

with S_f is the fiber cross-sectional area.

The maximum force F_{max} is given by one of the following conditions, depending on the loading mode:
$\frac{dF}{d\sigma} = 0$ (stable failure under deformation-controlled conditions)
$\alpha = \alpha_c$ (unstable failure under load-controlled conditions)
The first condition of stable failure yields

$$\sigma_{max} = \sigma_0\left(m\frac{V}{V_0}\right)^{-\frac{1}{m}} \tag{1.16}$$

$$\alpha(\sigma_{max}) = 1 - \exp\left(-\frac{1}{m}\right) \tag{1.17}$$

$$F_{max} = F(\sigma_{max}) = N_t S_f \sigma_0\left(m\frac{V}{V_0}\right)^{-\frac{1}{m}} \exp - \frac{1}{m} \tag{1.18}$$

The second condition of unstable failure yields

$$F_{\max} = F(\alpha_c) = N_t S_f \sigma_F (1 - \alpha_c) \tag{1.19}$$

where σ_F is the strength of tow at instability. F_{max} corresponds now to tow ultimate strength. It can be shown that α_c is given by Equation (1.10), which implies that $\sigma_F = \sigma_{max}$. As a consequence, F_{max} is also given by Equation (1.15) in the presence of unstable failure. The only difference between both tow behaviors under load- or strain-controlled conditions lies in the post maximum force responses.

To estimate scattering of the maximum force F_{max}, the binomial function can be considered $B(N_t, \alpha(\sigma_{max}))$ (respectively, α_c), which is naturally equal to the critical number of broken fibers N_c (statistical definition):

$$N_c = B(N_t, \alpha(\sigma_{max})) \tag{1.20}$$

Thus, the expectation $E()$ and the variance $S^2()$ of the critical number of broken fibers N_c are deduced from the expectation and the variance of the binomial function, which finally yields the expectation and the variance of the maximum force F_{max}:

$$E(N_c) = N_t(\sigma_{max}) \Rightarrow E(F_{max}) = N_t(1 - \alpha(\sigma_{max}))S_f\sigma_{max} \tag{1.21}$$

$$S^2(N_c) = N_t(1 - \alpha(\sigma_{max}))\alpha(\sigma_{max}) \Rightarrow S^2(F_{max}) = (S_f\sigma_{max})^2 N_t(1 - \alpha(\sigma_{max}))\alpha(\sigma_{max}) \tag{1.22}$$

This allows calculation of the coefficient of variation C_v, given by Daniels [62], McCartney and Smith [66], and Gurvich and Pipes [67]:

$$C_V(F_{max}) = \frac{S(F_{max})}{E(F_{max})} = \sqrt{\frac{\alpha(\sigma_{max})}{N_t(1 - \alpha(\sigma_{max}))}} \tag{1.23}$$

An important consequence of Equation (1.23) is that the coefficient of variation is small when the total number of fibers N_t is high: $N_t \geq 500$ in most SiC fibers. Therefore, according to theory, the maximum force (tow strength) should not show variation. Experimental results are at variance with theory: an unpredicted scatter in SiC Nicalon and Hi-Nicalon tow strengths was observed (Figure 1.5). It was attributed to imperfect local load sharing caused by fiber interactions (such as friction) or dynamic effects due to individual fiber breaks. Imperfect load sharing induces a drop in tow strengths (Figure 1.6). Fiber stress redistribution depends on the degree of interaction of the broken fiber with its neighbors. Taking into account random local load sharing allowed sound predictions of tow strengths and of associated scatter [61].

Although tow strength data are influenced by extrinsic factors, testing of tows is an interesting technique to determine fiber properties [68–72].

1.4.2 Filaments–Tows Relations: Tow-Based Testing Methods for Determination of Single Filament Properties

It is worth pointing out that the critical number of fibers broken individually at maximum force determines tow strength:

$$\sigma(F_{max}) = \sigma(\alpha = \alpha_c) \tag{1.24}$$

whereas the average filament strength corresponds to the particular value $\alpha = 0.5$.

$$\overline{\sigma} = \sigma(\alpha = 0.5) \tag{1.25}$$

Since $\alpha_c < 0.5$, $\sigma(F_{max}) < \overline{\sigma}$ (Tables 1.3 and 1.5). Both strengths can be calculated using Equation (1.4) when m, σ_0, and V_0, are available. α_c is derived from m using Equation (1.10). When theoretical α_c is identical to the experimental value at F_{max}, this indicates that there was no fiber interaction during the tests (equal load sharing).

The failure characteristics of single filaments can be extracted from the tensile stress–strain curves determined on tows [68–72]. For this purpose, filament strengths are derived from the force and the effective bundle section,

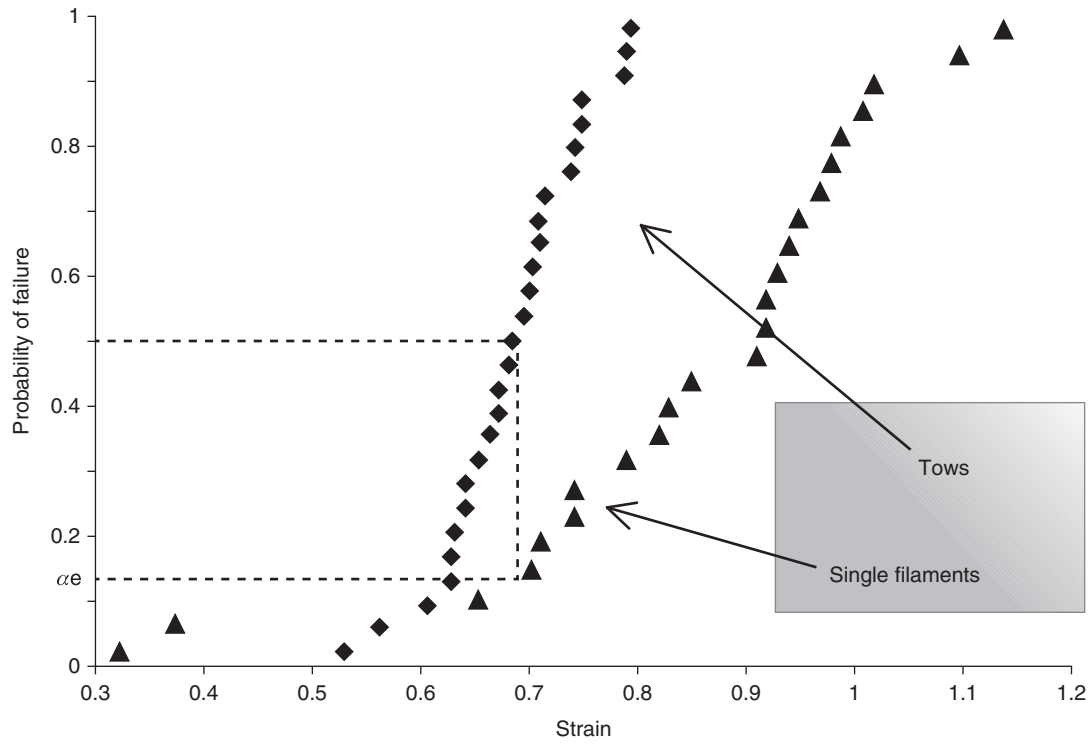

FIGURE 1.5
Statistical distributions of strains-to-failure for Nicalon SiC-based single filaments and multifilament tows.

taking into account the number of fibers broken individually. The number (j) of fibers broken at load F_j is derived from compliance C_j:

$$N_j = N_0(1 - C_0/C_j) \tag{1.26}$$

where N_0 is the initial number of intact fibers in the tow and C_0 is the corresponding compliance.

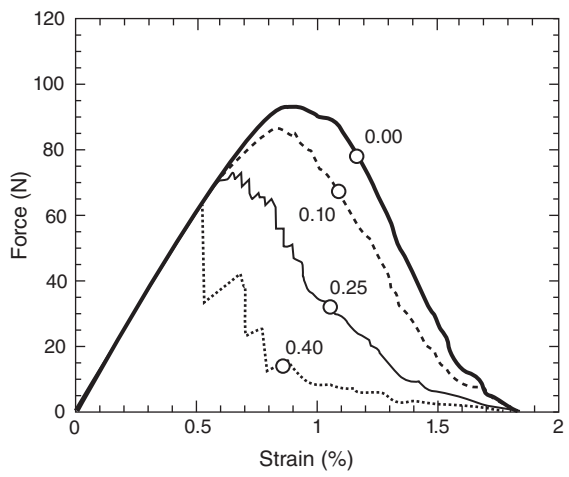

FIGURE 1.6
Influence of fiber interactions by random load sharing on the tensile load strain behavior of multifilament tows (predictions).

The estimator $P = N_j/N_0 = 1 - C_0/C_j$, can be used since the sample size is generally large, owing to the number of filaments present in a tow.

Deformation-based analysis should be preferred since measurement of fiber sections is not necessary (Figure 1.2). However, a sound method of strain measurement is required [71]. Then, deriving stresses on filaments from strains is straightforward when Young's modulus is available.

The tow testing technique is interesting because a significant sample size can be obtained using a single test. However, an artifact may result from fiber misalignment or fiber fractures during test specimen preparation. Specimen preparation and testing require much care. The degree of fiber interaction can be checked from the comparison of theoretical and experimental values of α_c. α_c data are reported in Table 1.5.

1.5 MECHANICAL BEHAVIOR AT HIGH TEMPERATURES

At intermediate temperatures <1000°C, most SiC-based fibers are sensitive to subcritical crack growth. Strength degradation of SiC single filaments starts at temperatures >1000°C [73,74], and creep at temperatures >1100°C [8]. It was also found that growth of a silica layer at fiber surface as well as oxygen diffusion is enhanced under load [75]. The intermediate temperature range has been investigated essentially on low oxygen content SiC fibers and on Nicalon fibers. Recent unpublished works on SiC fibers of first generation confirmed the phenomenon of subcritical crack growth. Oxide fibers have not been investigated whereas carbon fibers are consumed in the presence of oxygen at temperatures >400°C.

1.5.1 Strength Degradation and Oxidation at High Temperature

Non-oxide fibers experience oxidation-related effects in the high temperature range (above 900°C). However, this temperature may be lower for fibers that contain larger amounts of oxygen. Quite all the results found in the literature have been determined on single filaments. The authors were essentially interested in creep and strength retention after heat treatment or oxidation at high temperatures. The strength retention at room temperature generally decreases with increasing the heat treatment temperature [1,76,77] and the load [77]. At temperatures >1000°C, the oxidation was found to cause the growth of SiC grains, drop of resistivity, and degradation of strength for Nicalon and Hi-Nicalon fibers [76]. At all temperatures, the formation of a uniform silicon oxide layer at the surface of fibers has been observed. A very thin oxide film was formed at the temperatures between 650°C and 730°C [78].

Microstructure observations after heat treatments at 1300°C revealed that oxidation and loading accelerated new flaw nucleation and growth resulting in stress corrosion cracks in Hi-Nicalon fibers [77]. Oxidation in air at 800–1000°C only slightly decreased the strength of Nicalon fibers, whereas a decrease of strength and no noticeable change of the Young's modulus were reported for Tyranno fibers at lower temperatures (650–730°C) [78]. This strength decrease was related to flaw size increase after oxidation [78]. Hi-Nicalon single filaments retain >90% of their room temperature strength at 1300°C. By contrast, the strength data measured on multifilament strands show a steep decrease from 400°C. Yun and DiCarlo also reported strength data measured on Hi-Nicalon tows at high temperatures in air [79]. They found that tensile strength degradation started at 300°C. This phenomenon results from fiber bonding by a SiO_2 layer that grows at the surface of fibers.

E. Lara Curzio modeled the effect of oxidation on the stress–rupture time behavior of fiber bundles and composites [80,81]. The delayed failure of fiber bundles was attributed to formation of a silica layer on the surface of fibers; the thickness of this layer was introduced in place of critical flaw size in the linear fracture mechanics equation of strength leading to a fiber bundle strength decrease with time as $t^{-1/4}$ [80,81], which corresponds to a fiber independent stress exponent $n = 4$.

1.5.2 Static Fatigue Under Constant Load at Intermediate Temperatures: Subcritical Crack Growth

Several researchers have demonstrated since the 1960s the sensitivity of refractory materials to slow (subcritical) crack growth. Slow crack growth leads to failure, which implies that the strength is also time dependent.

1.5.2.1 Stress–Rupture Time Diagrams Delayed failure is indicated by finite rupture times under stresses much smaller than the failure stress (Figures 1.7–1.9) [82–84]. The rupture times generally decrease when the stresses are

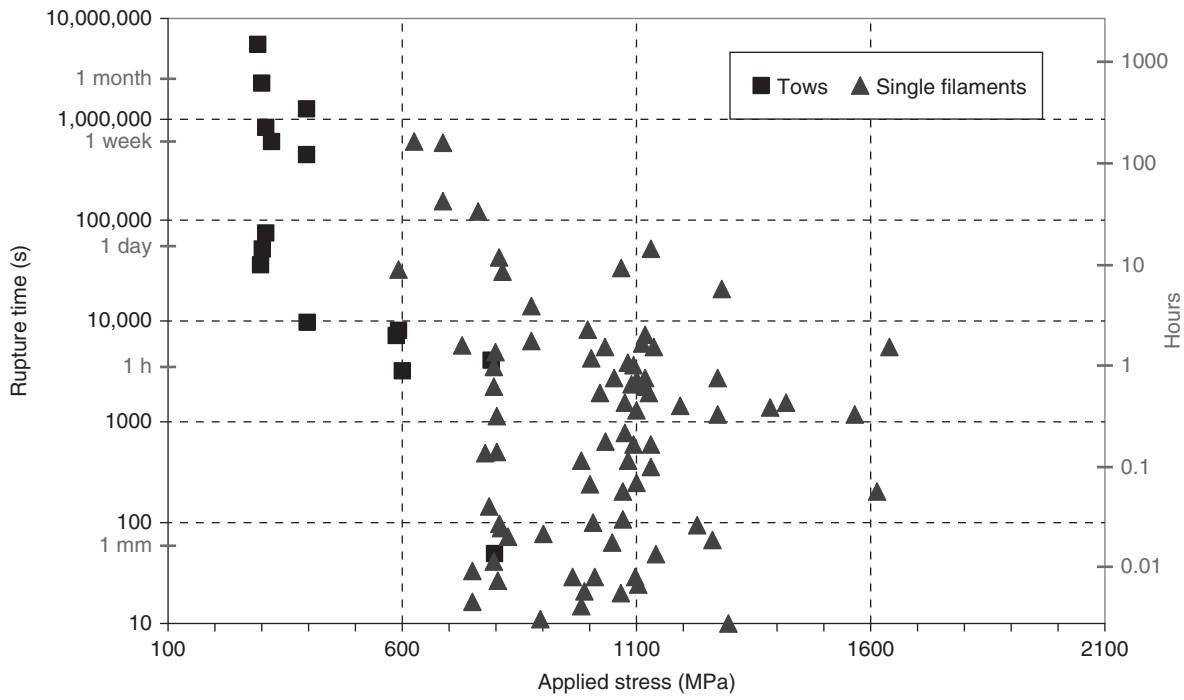

FIGURE 1.7

Stress–rupture time data determined on single SiC-based filaments (Hi-Nicalon) at 800°C. From Journal of the American Ceramic Society, March 2009.

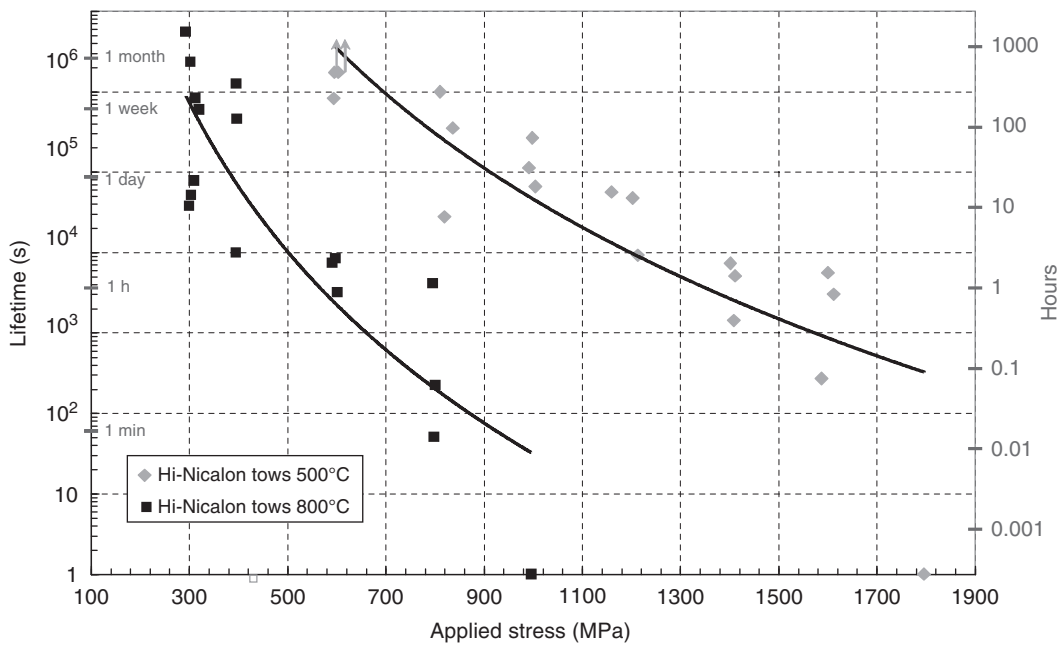

FIGURE 1.8

Stress–rupture time diagrams for Hi-Nicalon multifilament tows tows at 500°C and 800°C. From Journal of the American Ceramic Society, March 2009.

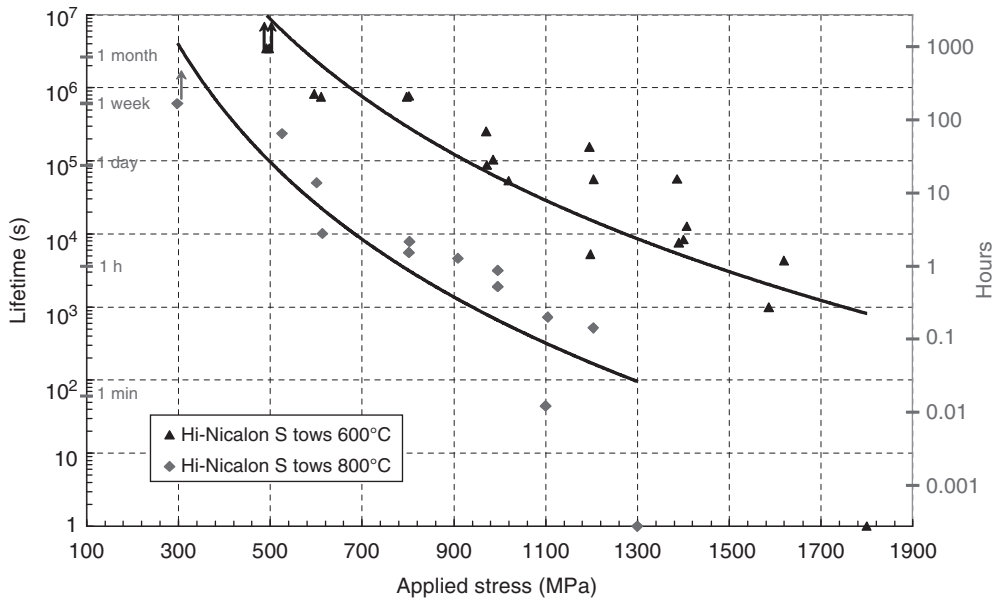

FIGURE 1.9
Stress–rupture time data for Hi-Nicalon S fiber bundles at 500°C and 800°C. From Journal of the American Ceramic Society, March 2009.

increased. Lifetimes of single filaments exhibit a significant scatter (Figure 1.7). The statistical variability at constant stress is similar to that one observed with ceramics when various specimens are tested. It results from the presence of flaws with different sizes.

The stress–rupture time data obtained for tows align on a curve that is fitted by the following power law (Figures 1.8 and 1.9):

$$t\sigma^n = A \tag{1.27}$$

where t is the rupture time, σ is the applied stress, n and A are constants depending, respectively, on material and environment.

This power law often describes nonlinear time-dependent responses such as that one dictated by slow crack growth activated by the environment under low stresses in ceramics [85]. The stress–rupture time behavior of tows must be regarded as a remarkable feature since it is at variance with that dispersed one of ceramics and single fibers. The constant A depends on the initial flaw size. It takes the same value for those specimens that possess flaws with the same initial size [85]. The response of tows can be related to the critical fiber-dictated failure mode, as discussed in section 1.4.2. When α_c is a constant, the critical fibers correspond to identical initial flaw sizes.

A and n are estimated from the stress–rupture time diagram using a regression technique (Tables 1.6 and 1.7). Unlike A, the stress exponent n does not display significant temperature dependence. It seems to depend on fiber. Close values of n were estimated for a large spectrum of commercial SiC-based fibers (Tables 1.6 and 1.7).

TABLE 1.6 Main Static Fatigue Constants Estimated on Tows for Nicalon-Type Silicon Carbide-Based Fibers [21,75]

	Nicalon	Hi-Nicalon		Hi-Nicalon S	
T (°C)	600	500	800	600	800
n	7.3	8.4	8.3	7.2	7.2
A (MPa^n sec)	2.10^{24}	$1.05.10^{30}$	$3.36\ 10^{26}$	$3.15.10^{26}$	$3.33.10^{24}$
E_a (KJ/mol)	140	185	185	177	177

TABLE 1.7 Main Static Fatigue Constants Estimated on Tows for Ube Silicon Carbide-Based Fibers at Various Temperatures [21]

	NL207		TS		TS11		Lox-M		ZMI	
T (°C)	n	$A \times 10^{25}$ (s MPa$^{7.3}$)	n	$A \times 10^{19}$ (s MPa$^{5.0}$)	n	$A \times 10^{21}$ (s MPa$^{5.8}$)	n	$A \times 10^{19}$ (s MPa$^{4.9}$)	n	$A \times 10^{31}$ (s MPa$^{9.1}$)
350	–	–	–	600	–	–	–	–	–	–
400	–	–	5.59	200	–	–	–	1 200	9.99	10 000
450	–	1 000	5.59	80	6.87	400	–	20	9.99	2 000
500	6.92	400	4.81	38	5.34	80	4.67	80	11.35	300
550	7.66	40	5.26	17	4.68	30	5.49	20	9.24	60
600	–	60	4.84	6.0	5.48	20	5.17	1.8	8.37	6.0
650	7.05	15	4.34	0.80	6.81	4.0	4.25	0.40	8.71	0.70
750	7.63	1.0	5.29	0.50	–	2.0	–	0.10	8.39	0.30
850	7.25	0.30	–	0.20	–	1.0	–	0.10	9.16	0.12
$\bar{n}$	**7.3**		**5.0**		**5.8**		**4.9**		**9.1**	

1.5.2.2 Mechanism of Slow Crack Growth Figure 1.10 demonstrates that oxygen is responsible for the delayed failure of fibers at high temperature under a stress far smaller than the failure stress. In pure nitrogen atmosphere, failure did not occur (the tests were interrupted after 1 month) whereas rupture time decreased to a plateau with increasing oxygen concentration. Above 15–20%, oxygen was in excess for the chemical reactions.

The following typical features were identified by SEM on the fracture surface of fibers (Figures 1.11 and 1.12):

- successive marks, indicative of slow crack growth;
- and a thin film of oxide on the external surface. The thickness of this film was generally quite small after tests lasting not more than 2 or 3 months. This duration is reasonable for practical reasons.

The delayed failure of SiC-based fiber bundles at temperatures below 800°C results from the subcritical crack growth of the surface defects by the oxidation of free carbon at grain boundaries and of the SiC nanograins or silicon oxicarbide at crack tip (Figure 1.13) [75]. Both phenomena may contribute simultaneously (Nicalon fibers) or sequentially (Hi-Nicalon S and SA3 fibers, which contain little free carbon not connected). Growth of a silica layer at fiber surface is not responsible for fracture. In the presence of free carbon, the crack length increase is attributed to the consumption

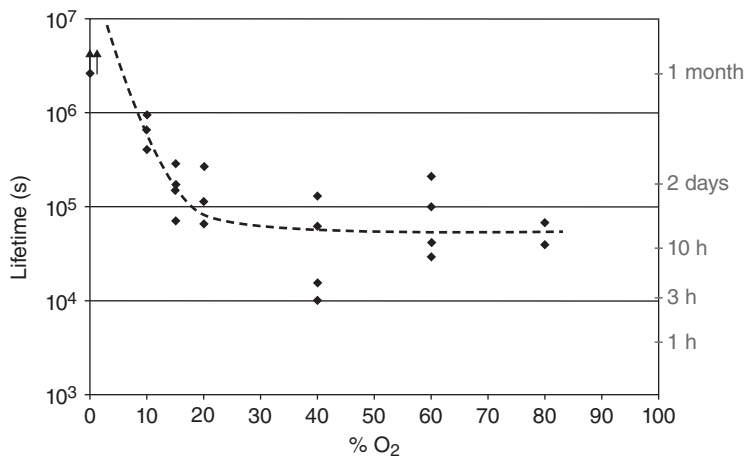

FIGURE 1.10

Influence of oxygen content on the rupture time of Hi-Nicalon fiber bundlles at 500°C under 1000 MPa. From Journal of the American Ceramic Society, July 2009.

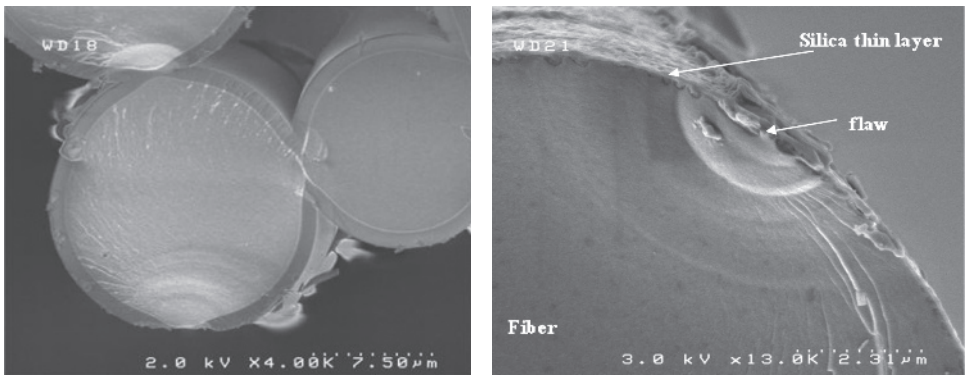

(a) (b)

FIGURE 1.11

SEM micrographs showing evidence of slow crack growth and oxide layer after static fatigue on (a) Hi-Nicalon fibers under 250 MPa at 1000°C during 13 days. (b) Nicalon fibers under 540 MPa at 700°C during 4 hours. From Journal of the American Ceramic Society, July 2009.

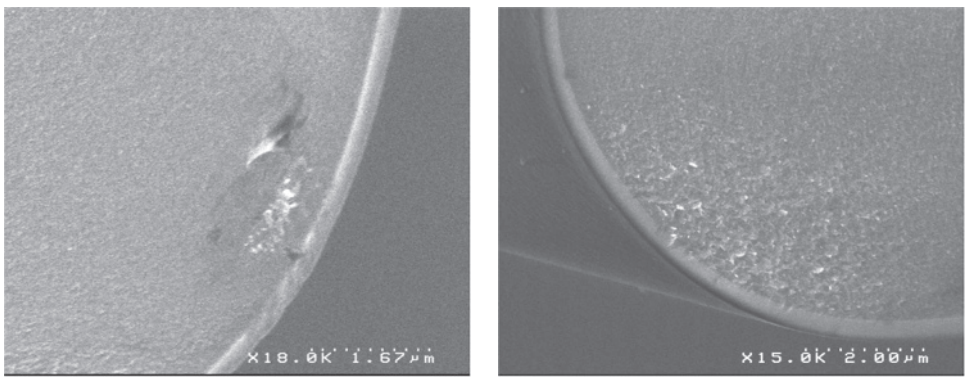

FIGURE 1.12

Typical examples of oxide layers observed at the surface of Nicalon fibers after static fatigue at 800°C under 300 MPa during ~2 months. From Journal of the American Ceramic Society, July 2009.

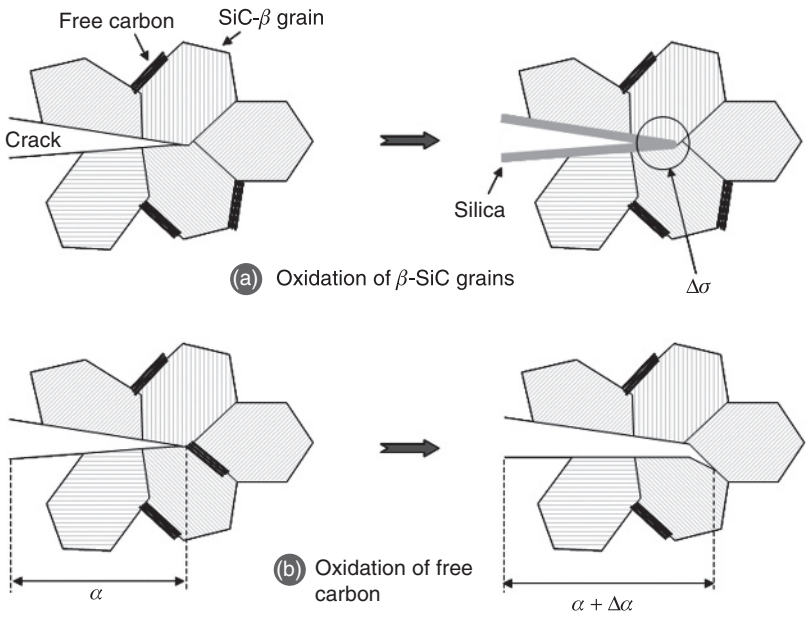

FIGURE 1.13

Schematic diagrams showing the mechanisms of slow crack growth at high temperature in air. From Journal of the American Ceramic Society, July 2009.

of free carbon. In the presence of silicon carbide or silicon oxicarbide, the silicon oxide formed at the defect/crack tip causes local volume increase (by 2.1 for SiC and less for SiO_xC_y), which induces a tensile stress $\Delta\sigma$. Those fibers with the largest fractions of free carbon are the least resistant to static fatigue:

Tyranno SA3 ≈ Hi-Nicalon S < Hi-Nicalon ≈ Nicalon
(≈ 2 at.%) (≈ 3 at.%) < (≈ 17 at.%) (≈ 15at.%): atomic concentrations of free carbon.

- Nicalon fiber contains large amounts of very reactive free carbon (≈15 at.%), and very small β-SiC nanograins (∼5 nm) embedded in silicon oxicarbide. These elements are very sensitive to oxidation due to their structure (free carbon) or their size; Valhas and Laanani demonstrated that smaller are the grains, the faster they oxidize [86]. In consequence both mechanisms can operate simultaneously and this is consistent with the small resistance to fatigue of this fiber.
- Hi-Nicalon fiber is essentially made of bigger β-SiC nanograins (∼10 nm) and a free carbon network (the electrical conductivity is high: about 70 S/m, compared to the Hi-Nicalon S and Nicalon fibers: 0.1 S/m). The oxidation of this network from the surface defects should be the predominant mechanism of slow crack growth. As a consequence, longer rupture times would be expected when compared to the Nicalon fibers.
- Hi-Nicalon S fiber contains much bigger β-SiC nanograins (∼20 nm) without the silicon oxicarbide, and a little free carbon located at grain boundaries and not connected. The oxidation of the β-SiC nanograins would contribute to slow crack growth. The resistance to static fatigue is greater than that of Hi-Nicalon fiber because free carbon is not connected and the SiC grains are bigger.
- Tyranno SA3 fiber possesses the same amount of free carbon in the surface as the Hi-Nicalon S fiber, but the difference lies in the SiC grain size: 50–100 nm vs. 20 nm for the Hi-Nicalon S fiber. The longer rupture times exhibited by the SA3 fiber can be attributed to the presence of much bigger grains, which oxidize more slowly than the smaller ones present in the other SiC-based fibers [51]. In this case the oxidation rate of the SiC grains would determine slow crack growth. Both phenomena of oxidation of SiC grains and free carbon may contribute sequentially to slow crack growth in the Hi-Nicalon S and Tyranno SA3 fibers.

Finally, the lifetime microstructure relationships can be highlighted by comparing rankings of resistances to static fatigue and microscopic features, which control the reactivity of constitutive elements:

Lifetime: Tyranno SA3 > Hi-Nicalon S > Hi-Nicalon > Nicalon
Free carbon: (≈ 2 at.%) (≈ 3 at.%) < (≈ 17 at.%) (≈ 15 at.%)
Grain size: (≈50–100 nm) (≈20 nm) > (≈10 nm) (≈5 nm)

In order to improve the fatigue resistance of these SiC-based fibers in air at intermediate temperatures between 400°C and 800°C, the manufacturers will have to reduce drastically the amounts of oxygen and free carbon near fiber surface and also to eliminate the surface defects, in order to limit the oxidation.

1.5.2.3 Model of Slow Crack Growth in Filaments Under a Constant Stress Models of slow crack growth have been proposed for engineering ceramics [85] and for tows [83]. The delayed failure of a single fiber is caused by the slow growth of a crack from an initial flaw size to a critical length. Crack growth rate is assumed to obey the following equation, which is usually employed to describe the slow propagation of cracks in fatigue in ceramics or metallic materials:

$$v = \frac{da}{dt} = A_1 K_I^n \tag{1.28}$$

where v is crack velocity, a is crack length, t is time, K_I is the stress intensity factor, and A_1 and n are constants depending, respectively, on environment and material.

Under constant stress σ, the lifetime of a single filament is the time period required for the particular flaw responsible for filament failure to grow from the initial size C_j to the critical length a_c:

$$t = \int_{C_j}^{a_c} \frac{da}{V} = \frac{2}{\sigma^n A_1 (n-2)} \left[\frac{C_j^{2-n/2}}{Y^n} - \frac{K_{IC}^{2-n} \sigma^{n-2}}{Y^2} \right] \tag{1.29}$$

where K_{IC} is the critical value of K_I (fracture toughness) and $Y = 2/\pi^{1/2}$ the geometrical parameter for a penny-shaped crack.

The initial flaw size C_j can be characterized by the tensile strength of the fiber, σ_f, in absence of environmental effects:

$$C_j = \frac{K_{IC}^2}{\sigma_f^2 Y^2} \tag{1.30}$$

Moreover, the filament failure strength distribution is described by the Weibull equation:

$$P(\sigma) = \alpha = 1 - \exp\left[-\frac{V}{V_0}\left(\frac{\sigma_f}{\sigma_{0f}}\right)^{m_f}\right] \tag{1.31}$$

where V_0 is the reference volume ($V_0 = 1\ m^3$) and m_f and σ_{0f} are the statistical parameters.

Inserting Equations (1.30) and (1.31) into (1.29) gives the following stress–rupture time relationship:

$$t = \frac{2}{Y^2 A_1 (n-2)\sigma^n}\left[\frac{\sigma_{0f}^{n-2}}{K_{IC}^{n-2}}\left[\frac{V_0}{V}\ln\frac{1}{1-\alpha}\right]^{\frac{n-2}{m_f}} - \frac{\sigma^{n-2}}{K_{IC}^{n-2}}\right] \tag{1.32}$$

A_1 can be expressed in terms of temperature T and the activation energy E_a related to the chemical reaction at crack tip:

$$A_1 = A_{10}\exp\left[-\frac{E_a}{RT}\right] \tag{1.33}$$

where A_{10} is constant and $R = 8.314$ J/K/mol.

Within the domain of low stresses, where the contribution of environment is effective, Equation (1.32) reduces to

$$t\sigma^n = A_0(\alpha)\exp\left[\frac{E_a}{RT}\right] = A(\alpha, T, E_a) \tag{1.34}$$

where

$$A_0(\alpha) = \frac{2}{Y^2(n-2)A_{10}}\left[\frac{\sigma_{0f}^{n-2}}{K_{IC}^{n-2}}\left[\frac{V_0}{V}\ln\frac{1}{1-\alpha}\right]^{\frac{n-2}{m_f}}\right] \tag{1.35}$$

Equations (1.34) and (1.35) show that A depends on fiber rank, temperature, and environment. Furthermore, it is worth emphasizing that the power law form of time to failure $t\sigma^n = A$ results from the use of power form for crack velocity (Equation 1.28).

1.5.2.4 Application to Static Fatigue of Tows Equations (1.32), (1.34), and (1.35) assume that fibers are subjected to stresses that remain constant during time. Lifetime of a tow is thus obtained for the particular value of α that corresponds to the critical fiber. The value of α may be equal to α_c determined under inert conditions or it may be smaller since all the filaments in a tow experience slow crack growth. But, this issue has not been examined yet.

For tows subjected to a constant load, the condition of constant stresses on filaments is not fulfilled because of reloading of surviving filaments at each filament failure from slow crack growth. As a consequence, the stresses on filaments increase step by step. The successive stresses and time steps can be determined to adapt Equations (1.32), (1.34), and (1.35) to the condition of constant load. In a first step, Equation (1.27) was used to extract slow critical crack growth constants from stress–rupture time diagrams, assuming that the stress on fibers was equal to the initial applied stress. It appeared that Equation (1.27) fitted satisfactorily the experimental stress–rupture time curves. It can

be considered that the obtained slow crack growth data are not intrinsic values pertinent to filaments, but instead they characterize the behavior of tows.

1.6 SUMMARY

Using continuous refractory fibers is the most efficient way to obtain strong and tough CMCs at high temperature. Owing to a wide variety of potential matrices, the fibers must meet several requirements. They must withstand the high temperatures required by composite processing above 1000°C. Their thermoelastic and fracture characteristics must match the matrix. Fiber resistance to fast or delayed fracture determines composite ultimate strength under monotonous or fatigue loading. Fiber strength degrades at high temperatures in air, as a result of various temperature-dependent phenomena like subcritical crack growth, creep, and oxidation.

Fast fracture data for filaments exhibit a statistical distribution that can be approximated by Weibull equation. However, they follow normal distribution, which can be determined safely on large sample size. The statistical parameters depend tremendously on the selection of samples. Tensile tests on tows with large amounts of filaments are appropriate to estimate reliable filament characteristics, provided filaments interactions during tests are not significant. Multifilament tows are fundamental entities in textile composites. They control ultimate failure and they determine scatter in composite strength. They exhibit a damage-tolerant behavior, which depends on statistical distribution of filament strengths. A critical filament having 15–20% failure probability in the distribution of reference strengths dictates their ultimate strength.

REFERENCES

1. A. R. Bunsell and A. Piant. A review of the development of three generations of small diameter silicon carbide fibers. *J. Mater. Sci.*, 41, 823–839 (2006).
2. B. Clauss. Fibers for ceramic matrix composites [Chapter 1], in *Ceramic Matrix Composites: Fibre-Reinforced Ceramics and Their Applications*, edited by W. Krenkel (Wiley-VCH, Weinheim, Germany, 2008), pp. 1–19.
3. G. Chollon, R. Pailler, R. Naslain, and P. Olry. Correlation between microstructure and mechanical behaviour at high temperatures of a SiC fibre with a low oxygen content (Hi-Nicalon). *J. Mater. Sci.*, 32, 1133–1147 (1997).
4. R. Pailler, J. Lamon, A. Guette, and I. Martin-Litas. Non-oxide ceramic fibres: relationships between nanostructure or composition and properties. *Ann. Chim. Sci. Mat.*, 30(6), 565–578 (2005).
5. K. A. Keller, G. Jefferson, and R. J. Kerans. Progress in oxide composites, *Ann. Chim. Sci. Mat.*, 30, 659–671 (2005).
6. K. A. Keller, G. Jefferson, and R. J. Kerans. Oxide–oxide composites, in *Handbook of Ceramics and Glasses*, edited by N. P. Bansal (Kluwer Academic Publishers, New York, 2005), pp. 377–421.
7. A. Bunsell. Oxide fibers, in *Handbook of Ceramics and Glasses*, edited by N. P. Bansal (Kluwer Academic Publishers, New York, 2005), pp. 3–31.
8. R. Bodet, X. Bourrat, J. Lamon, and R. Naslain. Tensile creep behaviour of a silicon carbide-based fibre with a low oxygen content. *J. Mat. Sci.*, 30, 661–677 (1995).
9. G. A. Budnitskii and N. N. Machalaba. Some research trends at the institute. *Fibre Chem.*, 33(2), 85–95 (2001).
10. A. R. Bunsell and M. H. Berger. *Fine Ceramic Fibres*. (CRC Press, 1999).
11. A. R. Bunsell and M.-H. Berger. Fine diameter ceramic fibres. *J. Eur. Ceram. Soc.*, 20, 2249–2260 (2000).
12. A. R. Bunsell. Fracture processes in fine silicon carbide fibers, in *Fiber Fracture*, edited by M. Elices and J. Llorca (2002), pp. 75–87.
13. A. R. Bunsell and J. Renard. *Fundamentals of Fibre Reinforced Composite Materials*. Series in Material Science and Engineering, Taylor & Francis Group (IOP Publishing Ltd., Bristol and Philadelphia, 2005).
14. S. M. Dong, G. Chollon, C. Labrugère, M. Lahaye, A. Guette, J. L. Bruneel, M. Couzi, R. Naslain, and D. L. Jiang. Characterization of nearly stoichiometric SiC ceramic fibres. *J. Mat. Sci.*, 36, 2371–2381 (2001).
15. T. Ishikawa. Recent developments of the SiC fiber Nicalon and its composites, including properties of the SiC fiber Hi-Nicalon for ultra-high temperature. *Compos. Sci. Technol.*, 51, 135–144 (1994).
16. R. E. Jones, D. Petrak, J. Rabe, and A. Szweda. Sylramic SiC fibers for CMC reinforcement. *J. Nucl. Mater.*, 283–287, 556–559 (2000).

17. K. Kumagawa, H. Yamaoka, M. Shibuya, and T. Yamamura. Thermal stability and chemical corrosion resistance of newly developed continuous Si-Zr-C-O Tyranno fiber. *Ceram. Eng. Sci. Proc.*, 18, 113–118 (1997).
18. K. Kumagawa, H. Yamaoka, M. Shibuya, and T. Yamamura. Fabrication and mechanical properties of new improved Si-M-C-(O) Tyranno fiber. *Ceram. Eng. Sci. Proc.*, 19, 65–72 (1998).
19. K. Kumagawa, H. Yamaoka, M. Shibuya, M. Suzuki, and T. Yamamura, Fabrication and mechanical properties of Si-M-C-(O) Tyranno fibers, *Ceram. Eng. Sci. Proc.*, 21(4), 291–298 (2000).
20. J. Lipowitz, J. A. Rabe, K. T. Nguyen, L. D. Orr, and R. R. Androl. Structure and properties of polymer-derived stoichiometric SiC fiber. *Ceram. Eng. Sci. Proc.*, 16(4), 55–62 (1995).
21. S. Mazerat. Fibres de renfort pour composites SiC/SiC: amélioration et corrélation de la durée de vie sous air à T<900°C avec la réactivité chimique (Fibres for reinforcement of SiC/SiC composite: improvement of lifetime and correlation with chemical reactivity). Ph.D. Thesis, No. 4554 (University of Bordeaux I, France, July 20, 2012).
22. G. Puyoo. Augmentation de la durée de vie de composites à matrice céramique: rôle des fibres Si-O-C et des interphases B-C-N (Improvement of lifetime for ceramic matrix composites: role of Si-O-C fibres and B-C-N interphases). Ph.D. Thesis, No. 4497, (University of Bordeaux I, France, March 9, 2012).
23. G. Simon and A. R. Bunsell, Mechanical and structural characterisation of the Nicalon silicon carbide fibre. *J. Mater. Sci.*, 19, 3649–3657 (1984).
24. Tyranno Fiber, Ube Industries, 1978-10, Kogushi, Ube City, Japan.
25. A. Hasegawa, A. Kohyama, R. H. Jones, L. L. Snead, B. Riccardi, and P. Fenici. Critical issues and current status of SiC/SiC composites for fusion. *J. Nucl. Mater.*, 283–287, 128–137 (2000).
26. C. Sauder. Effet de l'irradiation sur le comportement des fibres de carbure de silicium. Internal report LCTS, SEMES-050001 (2004).
27. G. Chollon, R. Pailler, R. Canet, and P. Delhaes. Correlation between microstructure and electrical properties of SiC-based fibres derived from organosilicon precursors. *J. Eur. Ceram. Soc.*, 18, 725–733 (1998).
28. R. Sarrazin. Phénomène d'endommagement progressif des fibres SiC en fatigue statique aux températures intermédiaires. Internal report LCTS (2011).
29. T. Ishikawa, H. Ishikawa, and H. Teranishi. Strength and structure of SiC fiber after exposure to high temperature. *J. Mater. Sci.*, 36, 205–217 (1987).
30. J. A. DiCarlo, and H.-M. Yun. Non-oxide (silicon carbide fibers, in *Handbook of Ceramics and Glasses*, edited by N. P. Bansal (Kluwer Academic Publishers, New York, 2005), pp. 32–53.
31. H. M. Yun, J. C. Goldsby, and J. A. DiCarlo. Tensile creep and stress–rupture behavior of polymer derived SiC fibers, in *Advances in Ceramic-Matrix Composites II*, edited by J. P. Singh and N. P. Bansal (American Ceramic Society, Westerville, OH, 1995), pp. 17–28.
32. H. M. Yun and J. A. DiCarlo. Comparison of the tensile, creep, and rupture strength properties of stoichiometric SiC fibers. Report NASA/TM-1999-209284 (1999).
33. R. Bodet, X. Bourrat, J. Lamon, and R. Naslain Tensile creep behavior of a silicon carbide-based fiber with a low oxygen content. *J. Mater. Sci.*, 30 661–677 (1995).
34. J. A. DiCarlo and H. M. Yun. Microstructural factors affecting creep–rupture failure of ceramic fibers and composites. *Ceram. Trans.*, 99, 119–134 (1998).
35. C. Sauder and J. Lamon, The tensile creep behavior of SiC-based fibers with low oxygen content. *J. Am. Ceram. Soc.*, 90(4), 1146–1156 (2007).
36. J. Hayashi, C. F. Liaw, T. Matzuzawat, K. Okamura, I. M. Omori, and S. Yajima. Simple synthesis of the continuous SiC fiber with high tensile strength. *Chem. Lett.*, 551, (1976).
37. Y. Hasegawa, M. Iimura, and S. Yajima. Synthesis of continuous silicon carbide fibre. Part 2: conversion of polycarbosilane fibre into silicon carbide fibres. *J. Mater. Sci.*, 15, 720–728 (1980).
38. P. Le Costumer, M. Monthioux, and A. Oberlin. Mécanisme de dégradation d'une fibre Nicalon Série 200, in *Comptes Rendus des Journées AMAC-CODEMAC*, edited by R. Naslain, J. Lamalle, and J. L. Zulian (Bordeaux, France, 1990), pp. 43–53.
39. O. Greck, J. P. Viricelle, D. Bahloul-Hourlier, P. Goursat, M. Dalbin, S. Thomin, and A. M. Flank. SiC-based ceramic fibres: thermal stability and oxidation behaviour. *Key Eng. Mater.*, 132–136, 1950–1953 (1997).
40. H.-E. Kim, and A. J. Moorhead. Strength of Nicalon silicon carbide fibers exposed to high-temperature gaseous environments. *J. Am. Ceram. Soc.*, 74(3), 666–669 (1991).
41. R. Bodet, J. Lamon, N. Jia, and R. E. Tressler. Microstructural stability and creep behavior of Si-O-C (Nicalon) fibers in carbon monoxide and argon environments. *J. Mater. Sci.* 30, 2241–2253 (1995).
42. K. Igashira. Decomposition and oxidation resistance of Si-M(Ti, Zr)-C-O fibers at elevated temperature. *J. Am. Soc.*, 255–260 (2003).

43. C. D. Batich, G. J. Choi, M. D. Sacks, M. Saleem, and W. M. Toreki. Polymer-derived silicon carbide fibers with low oxygen content. *Ceram. Eng. Sci. Proc.*, 198–208 (1992).
44. G. Chollon, R. Pailler, R. Naslain, F. Laanani, M. Monthioux, and P. Orly. Thermal stability of a PCS-derived SiC fibre with a low oxygen content (Hi-Nicalon). *J. Mater. Sci.*, 32, 327–347 (1997).
45. K. Okamura, T. Shimoo, W. Takano, and Y. Katase. Carbon elimination by heat-treatment in hydrogen and its effect on thermal stability of polycarbosilane-derived silicon carbide fibers. *J. Mater. Sci.*, 204, 6243–6251 (2004).
46. M. Takeda, J. Sakamoto, A. Saeki, and H. Ichikawa. Mechanical and structural analysis of silicon carbide fiber Hi-Nicalon type S. *Ceram. Eng. Sci. Proc.*, 17(4–5) 35–42 (1996).
47. M. Takeda, A. Urano, J. I. Sakamoto, and Y. Imai. Microstructure and oxidative degradation behavior of silicon carbide fiber Hi-Nicalon type S. *J. Nucl. Mater.*, 258–263, 1594–1599 (1998).
48. K. Morishita, S. Ochiai, H. Okuda, T. Ichikawa, and M. Sato. Fracture toughness of a crystalline silicon carbide fiber (Tyranno-SA3®). *J. Am. Ceram. Soc.*, 89(8) 2571–2576 (2006).
49. H. M. Yun, J. A. DiCarlo, R. T. Bhatt, and J. B. Hurst. Processing and structural advantages of the Sylramic-iBN SiC fiber for SiC/SiC components. *Ceram. Eng. Sci. Proc.*, 24(4) 247–253 (2003).
50. K. Morishita, S. Ochiai, H. Okuda, T. Ishikawa, M. Sato, and T. Inoue. Fracture toughness of a crystalline silicon carbide fiber (Tyranno-SA3). *J. Am. Ceram. Soc.*, 89(8) 2571–2576 (2006).
51. Association Française de Normalisation [AFNOR] NF EN 1007-4: Advanced Technical Ceramics—Ceramic Composites—Methods of Test for Reinforcement—Part 4: Determination of Tensile Properties of Filaments at Ambient Temperature (2004).
52. J. Lamon. *Mechanics of Brittle Fracture and Damage: Statistical Probabilistic Approaches* (In French "Mécanique de la rupture fragile et de l'endommagement: Approches Statistiques-Probabilistes") (Editions Hermès-Lavoisier, Paris, France, 2007).
53. N. Lissart, and J. Lamon, Statistical analysis of failure of SiC fibres in the presence of bimodal flaw populations. *J. Mater. Sci.* 32, 6107–6117 (1997).
54. A. J. Eckel, and R. C. Bradt. Statistical analysis of failure of SiC fibres in the presence of bimodal flaw populations. *J. Am. Ceram. Soc.* 72(3), 455–458 (1989).
55. K. Goda, and H. Fukunaga. The evaluation of the strength distribution of silicon carbide and alumina fibres by a multi-modal Weibull distribution. *J. Mater. Sci.* 21, 4475–4480 (1986).
56. M. R'Mili, N. Godin, and J. Lamon. Flaw strength distributions and statistical parameters for ceramic fibers: the normal distribution. *Phys. Rev. E*, 85, 051106 (2012).
57. E. G. Stoner, D. D. Edie, and S. D. Durham. An end-effect model for the single-filament tensile test. *J. Mater. Sci.* 29, 6561–6574 (1994).
58. F. T. Peirce. Journal of the textile institute. *Transactions*, 17, 355 (1926).
59. B. Epstein. Application of the theory of extreme values in fracture problems. *J. Am. Stat. Assoc.*, 43(243), 403–412 (1948).
60. J. Lamon. A micromechanics-based approach to the mechanical behavior of brittle-matrix composites. *Comp. Sci. Technol.*, 61, 2259–2272 (2001).
61. V. Calard and J. Lamon. Failure of fibres bundles. *Comp. Sci. Technol.*, 64, 701–710 (2004).
62. H. E. Daniels. The statistical theory of the strength of bundles of threads I. *Proc. R. Soc. A*, 183, 405–435 (1945).
63. B. D. Coleman. On the strength of classical fibers and fibers bundle. *J. Mech. Phys. Solid*, 7, 60–70 (1958).
64. S. L. Phoenix and H. M. Taylor. The asymptotic strength distribution of a general fiber bundle. *Adv. Appl. Prob.*, 5, 200–216 (1973).
65. S. L. Phoenix. Probabilistic strength analysis of fiber bundles structures. *Fiber Sci. Technol.*, 7, 15–31 (1974).
66. L. N. McCartney and R. L. Smith. Statistical theory of the strength of fiber bundles. *ASME J. Appl. Mech.* 105, 601–608 (1983).
67. M. Gurvich and R. Pipes. Strength size effect of laminated composites. *Comp. Sci. Technol.*, 55, 93–105 (1995).
68. Z. Chi, T. W. Chou, and G. Shen. Determination of single fiber strength distribution from fiber bundle testing. *J. Mater. Sci.*, 19, 3319–3324 (1984).
69. N. Lissart and J. Lamon. Evaluation des propriétés de monofilaments à partir d'essais de traction sur mèches, in *Comptes-rendus des 9° Journées Nationales sur les Composites (JNC9)*, vol. 2, edited by J. P. Favre and A. Vautrin (AMAC, 1994), pp. 589–598.
70. M. R'Mili and M. Murat. Caractérisation des fibres par amélioration de l'essai sur mèche avec mesure directe de la déformation. *C. R. Acad. Sci.*, 324(6), 355–364 (1997).
71. M. R'Mili, T. Bouchaour, and P. Merle. Estimation of Weibull parameters from loose bundle tests. *Comp. Sci. Technol.*, 56, 831–834 (1996).
72. ENV1007-5: Advanced Technical Ceramics—Ceramic Composites—Methods of Test for Reinforcements—Part 5: Determination of Distribution of Tensile Strength and Tensile Strain to Failure of Filaments within a Multifilament Tow at Ambient Temperature (European Committee for Standardization, CEN TC 184 SC1, Brussels, Belgium, 1997).

73. M. Berger, N. Hochet, and A. R. Bunsell. Small diameter SiC-based fibers, in *Fine Ceramic Fibers*, edited by A. R. Bunsell and M. H. Berger (Marcel Dekker, New York, 1999), p. 265.
74. H. M. Yun and J. A. Di Carlo. Time/temperature-dependent tensile strength of SiC and Al_2O_3-based fibers. *Ceram. Trans.*, 74, 17–26 (1996).
75. W. Gauthier, F. Pailler, J. Lamon, and R. Pailler. Oxidation of silicon carbide fibers during static fatigue in air at intermediate temperatures. *J. Am. Ceram. Soc.*, 92(9), 2067–2073 (2009).
76. T. Shimoo, K. Okamura, and W. Mutoh. Oxidation behavior and mechanical properties of low-oxygen SiC fibers prepared by vacuum heat-treatment of electron-beam-cured poly(carbosilane) precursor. *J. Mater. Sci.*, 38, 1653–1660 (2003).
77. J. J. Sha, J. S. Park, T. Hinoki, and A. Kohyama. Tensile properties and microstructure characterization of Hi-Nicalon SiC fibers after loading at high temperature. *Int. J. Fract.*, 142, 1–8 (2006).
78. Y. Gogotsi and M. Yoshimura. Oxidation and properties degradation of SiC fibers below 850°C. *J. Mat. Sci. Lett.*, 13, 680–683 (1994).
79. H. M. Yun and J. A. Di Carlo. Thermomechanical behavior of advanced SiC fiber multifilament tows. *Ceram. Eng. Sci. Proc.*, 17(4), 61–67 (1996).
80. E. Lara-Curzio. Stress–rupture of Nicalon/SiC continuous fiber ceramic composites in air at 950°C. *J. Am. Ceram. Soc.*, 80 (12) 3268–3272 (1997).
81. E. Lara-Cuzio. Oxidation induced stress-rupture of fiber bundles. *J. Eng. Mater. Technol.*, 120, 105–109 (1998).
82. S. Bertrand, R. Pailler, and J. Lamon. Influence of strong fibre/coating interfaces on the mechanical behaviour and lifetime of Hi-Nicalon/$(PyC/SiC)_n$/SiC minicomposites. *J. Am. Ceram. Soc.*, 84(4), 787–794 (2001).
83. P. Forio, F. Lavaire, and J. Lamon, Delayed failure at intermediate temperatures (600°–700°C) in air in silicon carbide multifilament tows. *J. Am. Ceram. Soc.*, 87(5), 888–893 (2004).
84. W. Gauthier, and J. Lamon. Delayed failure of Hi-Nicalon and Hi-Nicalon S multifilament tows and single filaments at intermediate temperatures (500–800°C). *J. Am. Ceram. Soc.*, 92, 3, 702–709 (2009).
85. R. W. Davidge, J. R. McLaren, and G. Tappin. Strength-probability-time (SPT) relationships in ceramics. *J. Mater. Sci.*, 8, 1699–1705 (1973).
86. C. Valhas and F. Laanani. Thermodynamic study of the thermal degradation of SiC-based fibres: influence of grain size, *J. Mater. Sci. Lett.*, 14(22), 1558–1561 (1995).